Observation of asymmetric oxidation catalysis with B20 chiral crystals

Guowei Li*[a,b,c], Qun Yang[c], Kaustuv Manna[d], Yang Zhang[e], Hua Lv[c], Anastasios Markou[c], Yan Sun[c], and Claudia Felser*[c]

[a] CAS Key Laboratory of Magnetic Materials and Devices, and Zhejiang Province Key Laboratory of Magnetic Materials and Application Technology, Ningbo Institute of Materials Technology and Engineering, Chinese Academy of Sciences, Ningbo 315201, China

[b] University of Chinese Academy of Sciences, 19 A Yuquan Rd, Shijingshan District, Beijing 100049, China

[c] Max Planck Institute for Chemical Physics of Solids, 01187 Dresden, Germany

[d] Department of Physics, Indian Institute of Technology, New Delhi 110016, India

[e] Department of Physics, Massachusetts Institute of Technology, Cambridge, Massachusetts 02139, USA

Email: liguowei@nimte.ac.cn, claudia.felser@cpfs.mpg.de

ABSTRACT

Heterogeneous processes for enantiomeric processes based on inorganic crystals have been a topic of resurgent interest. However, it remains a challenge to answer the question of what the driving forces for the emergence of homochirality in nature and chemical reactions are. Here, we propose one possible driver of enantioselectivity, namely orbital angular momentum (OAM) polarization. Enantioselective recognition of 3,4-dihydroxyphenylalanine (DOPA) was achieved by using B20 group PdGa crystals with different chiral lattices. Orbital textures of PdGa enantiomers (namely PdGa-A and PdGa-B) suggest large OAM polarization for the bands near the Fermi level and carrying opposite signs. This leads to the difference in adsorption energy between PdGa chiral crystals and DOPA molecules, depending on the pairing ability between the O 2p and Pd 4d orbital. These results provide a new route to achieving enantioselectivity with pure inorganic crystals and may hold an answer to the origin of chirality in nature.

Introduction

When Louis Pasteur introduced the concept of molecular chirality in his groundbreaking work in 1848, he also questioned what might be the forces for the synthesis of the first asymmetric natural products.[1] A variety of strategies have been introduced over the last eighty years for the controlled synthesis and eventual separation of pure enantiomers, which provides a promising answer for the arising of life in the prebiotic stage.[2-5] Unfortunately, still, no consensus has been reached to uncover the most likely scenario of how the mirror symmetry is initially broken.

Inorganic solids such as minerals, metals, and semiconductors have invoked a popular research interest because they can obtain chirality from surface modification or external fields, and thus endow bioorganic molecules with homochirality.[6] Remarkably high activity and selectivity in enantiospecific separation and asymmetric reactions were reported on various solid catalysts such as Au, Pd, and Fe_3O_4.[7-9] This can be explained by either electronic structure chirality or crystal structure chirality. The former assumes that the spin-polarized electrons can be viewed as chiral particles longitudinally and could interact with adsorbed molecules according to the chiral-induced spin selectivity (CISS) mechanism.[10] The latter represents the chirality of the crystal surfaces when their Miller indices ($h\ k\ l$) obey $h \neq k \neq l \neq k$ and $h \times k \times l \neq 0$, for example, the (643) surface of cubic Pt.[11-12] However, little is known about the chemical effects of pure inorganic compounds with bulk chirality crystal structures.

Intermetallic compounds with the space group $P2_13$ such as PdGa, RhSi, and CoSi are promising candidates for the probing of chirality due to their exotic chemical and physical properties.[13-15] Taking PdGa as an example, at least three catalogs of chirality can be found in this family of compounds as a result of their noncentrosymmetric bulk structure. a) Bulk chirality. Pd and Ga atoms are helically stacked along the [111] polar direction, suggesting the existence of two enantiomers with reversed handedness of helices.[16] b) Surface chirality. For the threefold symmetric (111) surface of the B20 compounds, although the topmost layer of Pd atoms is achiral, the Pd and Ga trimers in the 2nd and 3rd outmost surface layers could induce surface chirality and then influence the surface properties of the outmost Pd layer.[17] c) Electronic structures chirality. Chiral fermions and chiral Fermi-arc surface states with reversal velocities are experimentally confirmed, which is closely related to the chirality of bulk structures.[18] Thus, it is not surprising that B20 compounds such as PdGa have been explored a long time ago as heterogeneous catalysts.[19] The chiral Fermi-arc surface states serve as catalytic active sites and provide stable electron baths for redox reactions.[20] More importantly, enantioselective adsorption and elimination reaction towards prochiral molecules has been achieved on the (111) surface due to the different surface termination and the surface chirality originating from the second outmost surface layers.[21-22] With these experimental facts in mind, it is interesting to ask the question of whether the bulk crystal chirality initiates the enantioselective reactions.

In this work, we proposed that the intrinsic OAM polarization induced by the bulk chirality can drive the enantioselective reactions. We successfully obtained two PdGa bulk crystals with opposite chiralities and then studied their response toward the oxidation of DOPA enantiomers. It is found that the electro-oxidation of L-DOPA and D-DOPA is strongly dependent on the bulk chirality of PdGa crystals. The difference in oxidation behaviors can be explained by the classical thermodynamic adsorption theories, with the adsorption energies of L- and D-DOPA being different at the same crystal surface of PdGa. To understand the origin of adsorption differences, we performed a theoretical

investigation on the PdGa crystals and found the existence of strong OAM polarizations, with their signs being chiral-dependent. Considering the mirror-symmetric orbital polarization of O *2p* orbital in DOPA, we believed that the enantioselective adsorption of DOPA is driven by the polarization mismatch between the DOPA adsorbates and PdGa substrate. Our work suggests that the enantioselective reactions could happen on pure crystals without any surface modification, which provides a potential strategy for asymmetric synthesis on pure inorganic crystals or minerals.

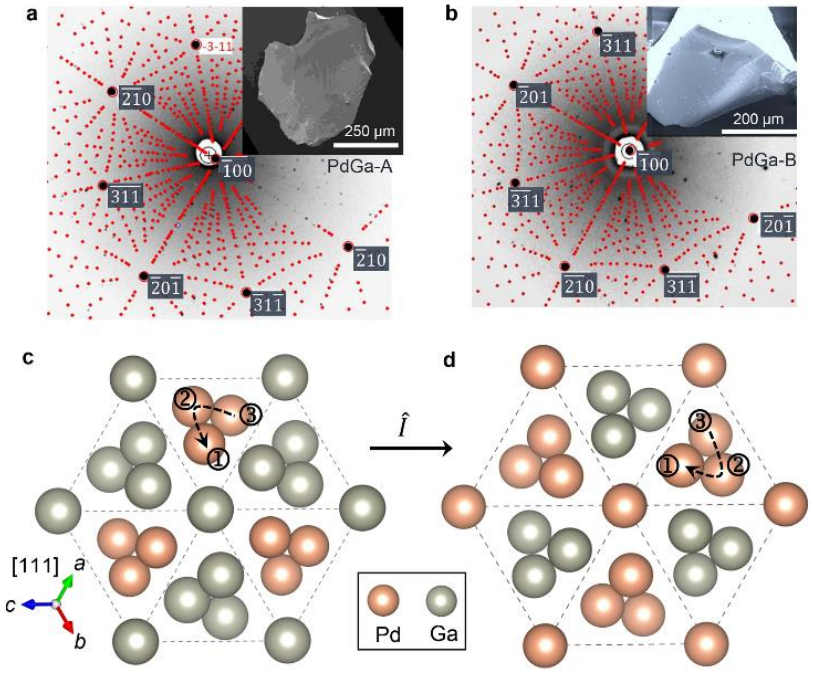

Fig. 1. a. The Laue diffraction pattern for PdGa-A crystal, with Pd at x = 0.14220, and Ga at x = 0.84270. The inset shows the SEM image of the single crystal used in this work. **b.** The Laue diffraction pattern for PdGa-B crystal, with Pd at x = 0.85780, and Ga at x = 0.15730. The handedness can also be seen from the corresponding low-energy electron diffraction (LEED) patterns.[18] **c.** Crystal structure of PdGa enantiomer A using the deposition number of CSD-1999938. **d.** Crystal structure of PdGa enantiomer B using the deposition number of CSD-1999942. The number 1 to 3 represent the Pd atoms positioned in the first, second, and third layers along the [111] direction.

Results and Discussion

Single crystallinity of the as-grown PdGa crystals was first analyzed using a white beam backscattering Laue X-ray diffraction at room temperature. Both the PdGa crystal batches show sharp and well-defined Laue spots, which can be indexed with a single pattern (Fig. 1a and b). This illustrates the excellent quality of the grown crystals. Then rigorous single-crystal X-ray diffraction was performed to analyze the structural chirality, Flack's parameter, etc. as explained in previous references [14, 18]. The identified enantiomers of form-A and form-B of the PdGa crystals are as defined in Ref.[23]. Two of the crystals obtained from the same batch were selected and served as the working electrode for DOPA

enantiomeric recognition. The scanning electron microscope (SEM) images recorded with secondary and backscattered electrons suggest the high homogeneity of the two crystals (inset Fig.1a-b, Fig. S1-2). The molar ratio of Pd and Ga is determined to be 1 according to the elemental analysis (Fig. S3). The entire refined crystallographic information along with final results are compiled in standard .cif format and can be retrieved from (https://www.ccdc.cam.ac.uk/structures/), using the deposition numbers CSD-1999938 to CSD-1999942. The detailed crystal structures were displayed in Fig. 2c-d. Both PdGa-A and PdGa-B crystals are crystallizing in the FeSi type of structure without the mirror and inversion symmetries. In the same as other B20 chiral compounds,[24] the intrinsic bulk chirality of PdGa is determined by the arrangement of Pd and Ga chiral motifs along the [111] direction. For A-type chirality PdGa crystal, Pd atoms are anti-clockwise stacked along the polar [111] direction, while Ga atoms are clockwise arranged. For B-type chirality, Pd and Ga atoms are stacked with an inverse sequence.[16] Here we must point out that the definition of chirality for PdGa is different from the previously reported method,[22, 25], where the surface chirality is derived from the different (111) and ($\overline{1}\overline{1}\overline{1}$) termination that cutting from a same crystal (*Note: The chirality comes from the surface termination, rather than bulk symmetry*).

As a proof-of-principle demonstration, DOPA molecules with different chirality are selected for the electrochemical recognition measurements. The oxidation behavior of DOPA molecules has been well documented at the surface of various solid electrodes, which makes the understanding of our data easier and more consolidated.[26-28] At first, cyclic voltammetry (CV) curves were recorded to confirm the happening of DOPA oxidation with PdGa-A as the working electrode. In the absence of L-DOPA (Fig. 2a), the broad oxidation peak between 0.6 and 1 V *vs*. Ag/AgCl can be attributed to the formation of Pd-O or Pd-OH bonding.[29] The strong reduction peak between 0 - 0.3 V can be indexed to the strong H adsorption process at the surface of Pd-based compounds.[30] When 4 mM of L-DOPA was introduced into the solution, a strong oxidation peak is observed at around 0.78 V, suggesting the oxidation of L-DOPA at the crystal surface.[28, 31] Other investigated samples including PdGa-B and Pt films exhibit the same behaviors towards DOPA oxidation (Fig. S4-5). As a comparison, 2H-MoS_2 single crystals can not drive the oxidation reaction because the (001) basal planes are catalytically inert to electrochemical reactions.[32] As a result, no oxidation peaks are found under the same measurement condition in the presence of DOPA (Fig. S6).

The limitation of the CV technique is the existence of a strong non-Faradic capacitive current, which makes the distinction of DOPA oxidation currents difficult. To increase the sensitivity of the chirality-dependent oxidation signal, the differential pulse voltammetry (DPV) technique is employed. We first recorded the DPV curves with PdGa-A crystal in the electrolyte with and without L-DOPA

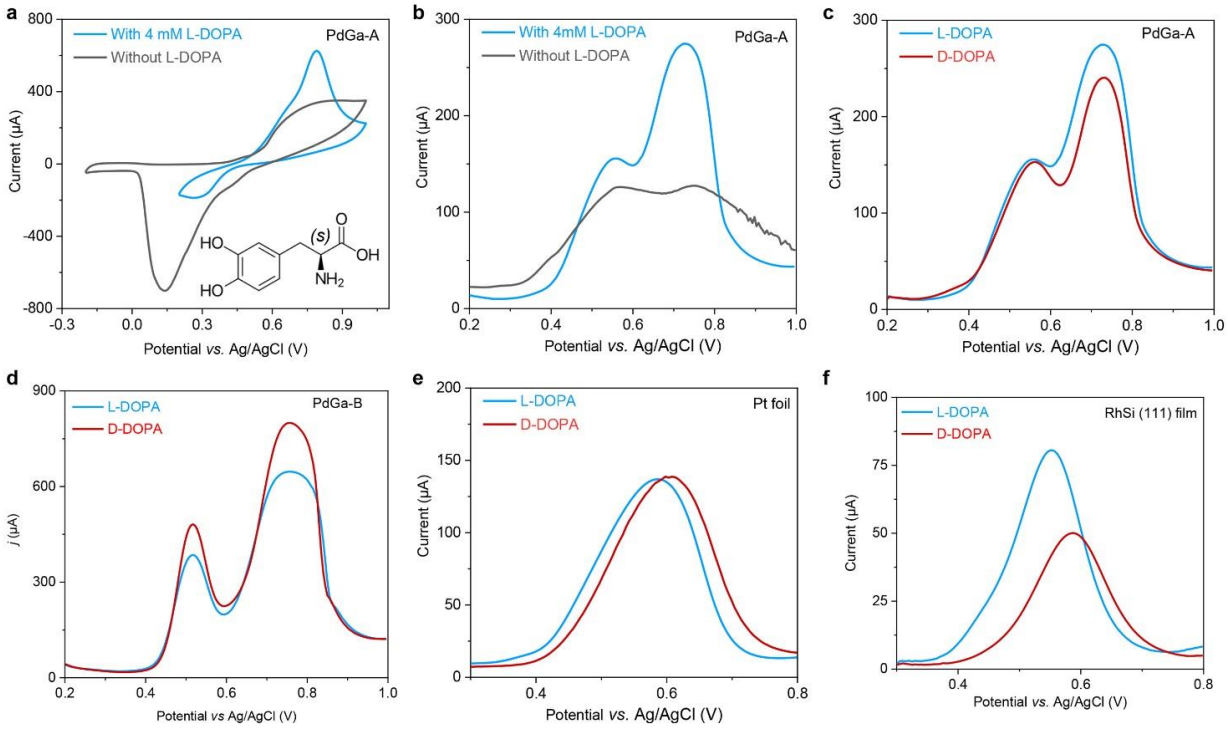

Fig. 2. a. CV profiles of PdGa-A crystal in the electrolytes with and without L-DOPA. The molecular structure of L-DOPA is shown inset. **b.** The corresponding DPV curves with and without L-DOPA. The peak at around 0.72 V can be attributed to the oxidation of DOPA. **c.** DPVs of DOPA enantioselective oxidation at the surface of PdGa-A (**c**) and PdGa-B (**d**) crystals. The oxidation of L-DOPA is more favorable than D-DOPA at the surface of PdGa-A, while the tendency is inversed with PdGa-B crystal. **e.** DPV curves at the surface of archival Pt foil. There is no difference between the oxidation of DOPA enantiomers. **e.** DPV curves at the surface of RhSi (111) thin films with a thickness of 40 nm. The enantioselective oxidation is more pronounced if only the (111) surface is exposed.

(Fig. 2B). One can see clearly the strong and well-defined DOPA oxidation peak at around 0.72 V. On the other hand, there are no significant changes for the peak corresponding to the formation of Pd-O and Pd-OH bonding at the lower potential of about 0.51 V. These features are fully consistent with the CV scanning results. The same results are found when the PdGa-B crystal was used (Fig. S7). This uncourtly confirmed the oxidation of DOPA at the surface PdGa crystals. Next, we measured the chirality-dependent oxidation of DOPA with PdGa-A and B crystals, respectively. As summarized in Fig. 2c-d, the oxidation currents for L-DOPA and D-DOPA are inversed at the surface of PdGa-A and PdGa-B crystals. In other words, the oxidation of L-DOPA at the surface of PdGa-A crystal is more favorable than D-DOPA, while PdGa-B crystal prefers the oxidation of D-DOPA. These results suggest that the oxidation of DOPA enantiomers is strongly dependent on the chirality of the PdGa crystals because all the other experimental details are kept the same. As an additional testimony, DOPA oxidation behaviors at the surface of archival Pt foil were recorded (Fig. 2e). There is no sign of

enantiomer selectivity from the identical oxidation currents, which is consistent with previous studies.[27] (*Note: the potentials for DOPA oxidation are strongly dependent on the electrode properties and measurement conditions. The theoretical standard electrode potential of DOPA oxidation is 0.75 V vs RHE.[33] The experimental values under acidic conditions are 0.76 V for Pt,[27] 0.82V for glassy carbon,[26] 0.85 V for Au electrode, 0.89 V for homocysteine modified Au electrode,[28], and 1.01 V for 2,20-Bis[2-(5,20-bithienyl)]-3,30-bithianaphthene oligomers coated glassy carbon[26]*)

Although the discrimination between two DOPA enantiomers is available with the bulk PdGa single crystals, the differences are not that so pronounced. This may be caused by two reasons. First, side reactions such as PdGa oxidation and radical adsorption happen in the potential window of DOPA oxidation (0.6-1 V *vs* RHE), which will influence the resolution. Second, besides the main surface of (111), other crystal surfaces and edges are inevitable for the investigated PdGa bulk crystals. This will make the determination of the DOPA oxidation currents more challenging. Wo notice that for the cubic B20 binary crystals with space group 198, the threefold rotation symmetry is along the [111] direction, endowing the (111) surface with exotic electronic properties such as the circular photo-galvanic effect.[18, 34-35] Thus, it is expected that (111) surface polar surface should have the maximum response towards chiral molecules' adsorption and reaction.[21] With this in mind, one may expect enhanced enantioselectivity by only exposing the (111) chiral surface area. High-quality single-crystalline RhSi (111) thin films with a thickness of 40 nm were synthesized (Fig. S8). CV investigation confirmed the oxidation of both L- and D-DOPA (Fig. S9). As expected, DPV curves exhibited well-defined DOPA oxidation peaks at around 0.6 V, suggesting the high enantioselective recognition ability at the polar (111) surface (Fig. 2f).

Enantiomeric oxidation at the surface of solid crystal surfaces is a typical homogenous reaction process. Thus, the differences in oxidation selectivity should be reflected in the adsorption energies.[36] To answer this question, we investigated the adsorption behaviors of DOPA enantiomers at the (111) crystal surface by taking the PdGa-A crystal as a model. The three-dimensional structures of L-DOPA and D-DOPA are displayed in Fig. 3a. Under acidic conditions, both enantiomers have a hydrophobic catechol group, a positively charged amine group, NH_3^+, and a negatively charged carboxyl group, COO^-. In the presence of a solid surface, the preferred adsorption sites are the highly charged cationic metals due to the cation-π interactions according to previous studies.[37-38] This is further confirmed by the optimized adsorption geometry of the PdGa-A (111)-DOPA pairs using density functional theory (DFT) in this work. Both L-DOPA and D-DOPA are firmly adsorbed onto the Pd sites via the O atoms from the carboxyl group (Fig. 3b-d, Fig. S10). Such an adsorption geometry is consistent with the surface electronic structure of PdGa (111), where the Pd site is positively charged with higher valence states than Pd metal.[39] The bonding lengths of Pd-O are 2.24 and 2.29 Å for L-DOPA and D-DOPA,

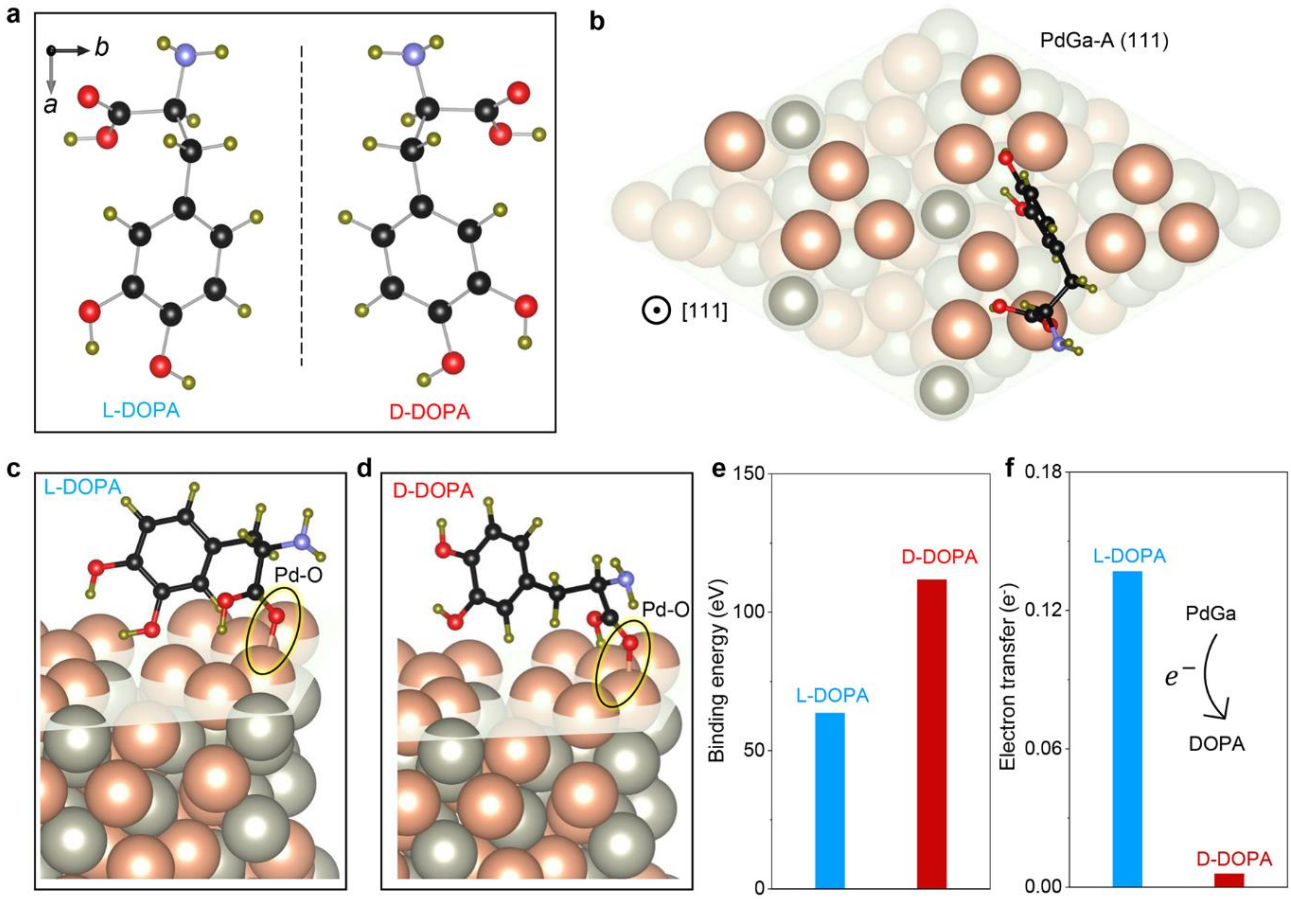

Fig. 3. a. The molecular structures of L- and D-DOPA ($C_9H_{11}NO_4$). The mirror plane is shown as the dashed line. The carbon connected with the amino and carboxylic acid group is the chiral center. Black, yellow, blue, and red spheres are C, H, N, and O atoms, respectively. **b.** Top view of the energetically favorable configuration for L-DOPA adsorbed on PdGa-A (111) surface. Brown spheres represent Pd atoms and grey for Ga atoms. DOPA prefer to stand on the surface and form bond with the top Pd atoms. Only the Pd atoms at the first layer and Ga atoms at the second layer are highlighted for a clear view of adsorption. Side view of the adsorption configuration of L-DOPA (**c**) and D-DOPA (**d**) at the surface of PdGa-A (111). In both cases, the bonds (highlighted in the black circle) are formed between the O atoms in the carboxylic acid (negatively charged) and the Pd atoms (positively charged) in the PdGa crystal. **e.** Adsorption energies (meV) of L- and D-DOPA adsorbed at the surface of PdGa-A (111). The energy difference is 48 meV, which is higher than the thermal energy at room-temperature (~25 meV). **f**. Charge transfer analysis at the interface of PdGa-A/DOPA pairs. Electrons are transferred from PdGa to DOPA, which is 0.137 e^- for L-DOPA and 0.006 e^- for D-DOPA.

respectively, which fall in the range of hydrogen bonding,[40] but much longer than the bonds between metals and oxygen intermediates in other catalysis reactions such as oxygen evolution.[41] To give another perspective on the bonding strength of Pd-O, the binding energies between PdGa and DOPA are calculated (Fig. 3e). As expected, the binding energy between the PdGa-A/L-DOPA pair is 0.063 eV, which is higher than that for the PdGa-A/L-DOPA pair (0.112 eV). The adsorption energy difference between the two DOPA enantiomers is 48 mV, which is well above thermal energy at room-temperature (~25 meV). Furthermore, we found more electrons are transferred from PdGa to L-DOPA ($0.137e^-$) than to D-DOPA ($0.006e^-$) (Fig. 3f). These quantitative calculation results undoubtedly confirmed that the adsorption of L-DOPA enantiomer is more favorable than the D-DOPA at the surface of PdGa-A crystal, which leading to the observed higher oxidation current of L-DOPA.

Now we try to answer the question of why the bond formation is more favorable for L-DOPA at the PdGa-A surface. One of the promising answers is that the spin polarization of the electrons from PdGa may differ from the one from the adsorbates, which will induce differences in electron transfer efficiencies and bonding energies.[42] With this in mind, we calculated band dispersion and extracted the spin polarization (Sz) of the spin-angular momentum from the phase-dependent atomic-orbital projection of the Bloch wavefunction for both PdGa-A and PdGa-B (Fig. S11). We found six spin-spitted non-degenerate bands along the symmetry line Γ-R around the Fermi level, merging into three two-fold degenerate bands at the time-reversal invariant point Γ. Although the spin-resolved data confirm an opposite sign of Sz at $+k_y$ and $-k_y$ for the sub-spin splitting bands, all components of spin polarization vanish when summed up, thus vanishing the spin angular polarization along the [111] direction. Therefore, the role of spin polarization and spin-selected electron transfers can be neglected in our case.

Finally, we examined the momentum-space texture of the orbital-angular momentum around the Fermi level (Fig. 4a, b). It is surprised to see a global OAM (Lz) in the electronic wave functions. Different from the SAM, the spin-split branches suggest a parallel OAM between orbital polarization and the momentum, with the (Lz) always carrying opposite signs at the $+k_y$ and $-k_y$ points, respectively. Although the OAM energy is generally much weaker than SAM,[43] it is enough to interact with right or left circularly polarized light to give reasonable circular dichroism (CD) signals.[44] Moreover, our calculations show that L-DOPA and D-DOPA carry opposite OAM along the same momentum direction when projecting to the LUMO orbital (O $2p$) indicating that the movements of electrons along the [111] direction are following different helical wavefronts(Fig. 4c-d). This results in the change of the lowest unoccupied molecular orbital (LUMO) when forming bonding with PdGa.[45-46] Most importantly, the energy shift of LUMO is closely related to the sign of OAM or the chirality of the

PdGa. This will change the energy gap between the highest occupied molecular orbital (HOMO) and LUMO, resulting in the chirality-dependent binding energies of DOPA when forming antibonding states with O 2p orbitals. This will finally result in the enantiomeric adsorption and oxidation depending on the compatibility of the OAM with each other.

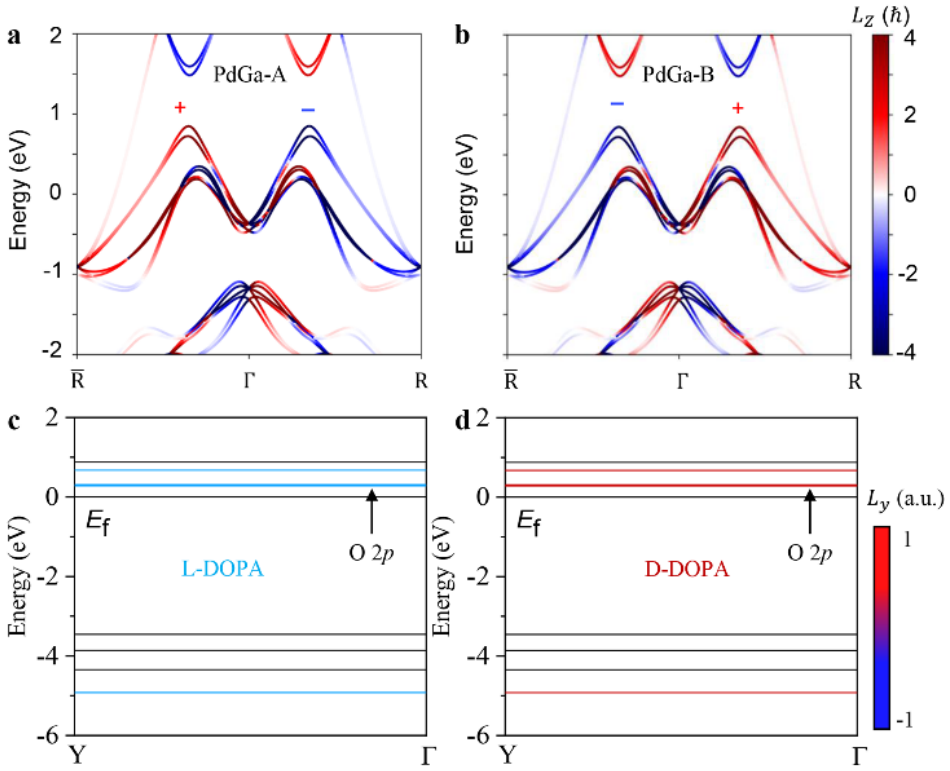

Fig. 4. The calculated orbital textures of PdGa-A (**a**) and PdGa-B (**b**) are projected on the orbital polarization (Lz) component. Lz exhibits opposite signs at $+k_y$ and $-k_y$ when considering the SOC effects, and are the OAM polarization is dependent on the chirality of PdGa. **c.** Orbital polarization of the O sites in L-DOPA. The O atom is the one that forms a bond with the Pd atom from PdGa. There is a strong polarization of the O 2p_y orbital at the LUMO level along the same momentum direction. **d.** The orbital polarization of O 2p_y in D-DOPA is reversed.

Conclusion

To conclude, it is demonstrated that enantiomeric recognition can be initiated by the intrinsic OAM polarization in the B20 family chiral compounds. This was experimentally confirmed by the different oxidation kinetics of DOPA enantiomers at the surface of PdGa (111) single crystals. Adsorption and bonds formed between the DOPA enantiomers and the chiral crystals are strongly dependent on the compatibility of the OAM with each other. Our study highlights the importance of OAM polarization as a promising driven force for enantiomeric recognition. It is hoped that this work will stimulate further studies of other solid states crystals (minerals), where more significant and pronounced enantiomeric recognition, enantiomer separation, and asymmetric catalysis reactions can happen.

Acknowledgements

This work was financially supported by the National Natural Science Foundation of China (Grant No. 52271194), the European Research Council (ERC Advanced Grant No. 742068 'TOPMAT'), DFG through SFB 1143 (project ID. 247310070), and the Würzburg-Dresden Cluster of Excellence on Complexity and Topology in Quantum Matter ct.qmat (EXC2147, project ID. 39085490) and via DFG project HE 3543/35–1, the Deutsche Forschungsgemeinschaft (Project-ID 258499086). G. Li thanks the support from the starting grant and the Foundation of the President of Ningbo Institute of Materials Technology and Engineering (NIMTE) of the Chinese Academy of Sciences (CAS).

Conflict of interests

The authors declare no conflict of interest.

References

1. Pasteur, L., Recherches sur les relations qui peuvent exister entre la forme cristalline, la composition chimique et les sens de la polarisation rotatoire. *Ann. Chim. Phys.* **1848,** *4*, 442-459.
2. Viedma, C.; Ortiz, J. E.; de Torres, T.; Izumi, T.; Blackmond, D. G., Evolution of solid phase homochirality for a proteinogenic amino acid. *J Am Chem Soc* **2008,** *130* (46), 15274-5.
3. Patel, B. H.; Percivalle, C.; Ritson, D. J.; Duffy, C. D.; Sutherland, J. D., Common origins of RNA, protein and lipid precursors in a cyanosulfidic protometabolism. *Nat. Chem.* **2015,** *7* (4), 301-7.
4. Bryliakov, K. P., Chemical Mechanisms of Prebiotic Chirality Amplification. *Research (Wash D*

C) **2020,** *2020*, 5689246.
5. Lorenz, H.; Seidel-Morgenstern, A., Processes to separate enantiomers. *Angewandte Chemie* **2014,** *53* (5), 1218-50.
6. Ma, W.; Xu, L.; de Moura, A. F.; Wu, X.; Kuang, H.; Xu, C.; Kotov, N. A., Chiral Inorganic Nanostructures. *Chem Rev* **2017,** *117* (12), 8041-8093.
7. Lieberman, I.; Shemer, G.; Fried, T.; Kosower, E. M.; Markovich, G., Plasmon-Resonance-Enhanced Absorption and Circular Dichroism. *Angewandte Chemie* **2008,** *120* (26), 4933-4935.
8. Hu, A.; Yee, G. T.; Lin, W., Magnetically recoverable chiral catalysts immobilized on magnetite nanoparticles for asymmetric hydrogenation of aromatic ketones. *J Am Chem Soc* **2005,** *127* (36), 12486-7.
9. Yutthalekha, T.; Wattanakit, C.; Lapeyre, V.; Nokbin, S.; Warakulwit, C.; Limtrakul, J.; Kuhn, A., Asymmetric synthesis using chiral-encoded metal. *Nat. Commun.* **2016,** *7*, 12678.
10. Gohler, B.; Hamelbeck, V.; Markus, T. Z.; Kettner, M.; Hanne, G. F.; Vager, Z.; Naaman, R.; Zacharias, H., Spin selectivity in electron transmission through self-assembled monolayers of double-stranded DNA. *Science* **2011,** *331* (6019), 894-7.
11. Shukla, N.; Gellman, A. J., Chiral metal surfaces for enantioselective processes. *Nat Mater* **2020,** *19* (9), 939-945.
12. Ahmadi, A.; Attard, G., Surface Reactivity at "Chiral" Platinum Surfaces. *Langmuir* **1999,** *15*, 2420-2424.
13. Yuan, Q. Q.; Zhou, L.; Rao, Z. C.; Tian, S.; Zhao, W. M.; Xue, C. L.; Liu, Y.; Zhang, T.; Tang, C. Y.; Shi, Z. Q.; Jia, Z. Y.; Weng, H.; Ding, H.; Sun, Y. J.; Lei, H.; Li, S. C., Quasiparticle interference evidence of the topological Fermi arc states in chiral fermionic semimetal CoSi. *Sci. Adv.* **2019,** *5* (12), eaaw9485.
14. Sessi, P.; Fan, F. R.; Kuster, F.; Manna, K.; Schroter, N. B. M.; Ji, J. R.; Stolz, S.; Krieger, J. A.; Pei, D.; Kim, T. K.; Dudin, P.; Cacho, C.; Widmer, R.; Borrmann, H.; Shi, W.; Chang, K.; Sun, Y.; Felser, C.; Parkin, S. S. P., Handedness-dependent quasiparticle interference in the two enantiomers of the topological chiral semimetal PdGa. *Nat. Commun.* **2020,** *11* (1), 3507.
15. Sanchez, D. S.; Belopolski, I.; Cochran, T. A.; Xu, X.; Yin, J. X.; Chang, G.; Xie, W.; Manna, K.; Suss, V.; Huang, C. Y.; Alidoust, N.; Multer, D.; Zhang, S. S.; Shumiya, N.; Wang, X.; Wang, G. Q.; Chang, T. R.; Felser, C.; Xu, S. Y.; Jia, S.; Lin, H.; Hasan, M. Z., Topological chiral crystals with helicoid-arc quantum states. *Nature* **2019,** *567* (7749), 500-505.
16. Armbrüster, M.; Borrmann, H.; Wedel, M.; Prots, Y.; Giedigkeit, R.; Gille, P., Refinement of the crystal structure of palladium gallium (1:1), PdGa. *Z. Kristallogr. NCS* **2010,** *225* (4), 617-618.
17. Prinz, J.; Groning, O.; Brune, H.; Widmer, R., Highly enantioselective adsorption of small prochiral molecules on a chiral intermetallic compound. *Angew Chem Int Ed Engl* **2015,** *54* (13), 3902-6.
18. Schroter, N. B. M.; Stolz, S.; Manna, K.; de Juan, F.; Vergniory, M. G.; Krieger, J. A.; Pei, D.; Schmitt, T.; Dudin, P.; Kim, T. K.; Cacho, C.; Bradlyn, B.; Borrmann, H.; Schmidt, M.; Widmer, R.; Strocov, V. N.; Felser, C., Observation and control of maximal Chern numbers in a chiral topological semimetal. *Science* **2020,** *369* (6500), 179-183.
19. Kovnir, K.; Armbrüster, M.; Teschner, D.; Venkov, T. V.; Jentoft, F. C.; Knop-Gericke, A.; Grin, Y.; Schlögl, R., A new approach to well-defined, stable and site-isolated catalysts. *Science and Technology of Advanced Materials* **2007,** *8* (5), 420-427.
20. Yang, Q.; Li, G.; Manna, K.; Fan, F.; Felser, C.; Sun, Y., Topological Engineering of Pt-Group-

Metal-Based Chiral Crystals toward High-Efficiency Hydrogen Evolution Catalysts. *Adv Mater* **2020,** *32* (14), e1908518.

21. Stolz, S.; Danese, M.; Giovannantonio, M. D.; Urgel, J. I.; Sun, Q.; Kinikar, A.; Bommert, M.; Mishra, S.; Brune, H.; Groning, O.; Passerone, D.; Widmer, R., Asymmetric Elimination Reaction on Chiral Metal Surfaces. *Adv. Mater.* **2021**, e2104481.

22. Yakutovich, A. V.; Hoja, J.; Passerone, D.; Tkatchenko, A.; Pignedoli, C. A., Hidden Beneath the Surface: Origin of the Observed Enantioselective Adsorption on PdGa(111). *J. Am. Chem. Soc.* **2018,** *140* (4), 1401-1408.

23. J. C. H. Spence; J. M. Zuo; M. O'Keeffe; Marthinsen, K.; Hoier, R., On the minimum number of beams needed to distinguish enantiomorphs in x-ray and electron diffraction. *Acta Cryst.* **1994,** (A50), 647–650

24. Daniel S Sanchez; Tyler A Cochran; Ilya Belopolski; Zi-Jia Cheng; Xian P Yang; Yiyuan Liu; Xitong Xu; Kaustuv Manna; Jia-Xin Yin; Horst Borrmann; Alla Chikina; Jonathan Denlinger; Vladimir N Strocov; Claudia Felser; Shuang Jia; Guoqing Chang; Hasan, M. Z., Helicoid-arc van Hove singularities in topological chiral crystals. *arXiv.2108.13957* **2021**.

25. Prinz, J.; Pignedoli, C. A.; Stockl, Q. S.; Armbruster, M.; Brune, H.; Groning, O.; Widmer, R.; Passerone, D., Adsorption of small hydrocarbons on the three-fold PdGa surfaces: the road to selective hydrogenation. *J. Am. Chem. Soc.* **2014,** *136* (33), 11792-8.

26. Arnaboldi, S.; Benincori, T.; Cirilli, R.; Kutner, W.; Magni, M.; Mussini, P. R.; Noworyta, K.; Sannicolo, F., Inherently chiral electrodes: the tool for chiral voltammetry. *Chem. Sci.* **2015,** *6* (3), 1706-1711.

27. Wattanakit, C.; Come, Y. B.; Lapeyre, V.; Bopp, P. A.; Heim, M.; Yadnum, S.; Nokbin, S.; Warakulwit, C.; Limtrakul, J.; Kuhn, A., Enantioselective recognition at mesoporous chiral metal surfaces. *Nat Commun* **2014,** *5*, 3325.

28. Takuya Nakanishi; Mariko Matsunaga; Makoto Nagasaka; Toru Asahi; Osaka, T., Enantioselectivity of Redox Reaction of DOPA at the Gold Electrode Modified with a Self-Assembled Monolayer of Homocysteine. *J. Am. Chem. Soc.* **2006,** *128* (41), 13322–13323.

29. Bhalothia, D.; Chou, J. P.; Yan, C.; Hu, A.; Yang, Y. T.; Chen, T. Y., Programming ORR Activity of Ni/NiO_x@Pd Electrocatalysts via Controlling Depth of Surface-Decorated Atomic Pt Clusters. *ACS Omega* **2018,** *3* (8), 8733-8744.

30. Kibler, L. A.; El-Aziz, A. M.; Kolb, D. M., Electrochemical behaviour of pseudomorphic overlayers: Pd on Au(1 1 1). *Journal of Molecular Catalysis A: Chemical* **2003,** *199* (1-2), 57-63.

31. Kang, Y. J.; Oh, J. W.; Kim, Y. R.; Kim, J. S.; Kim, H., Chiral gold nanoparticle-based electrochemical sensor for enantioselective recognition of 3,4-dihydroxyphenylalanine. *Chem. Commun.* **2010,** *46* (31), 5665-7.

32. Li, G.; Xu, Y.; Song, Z.; Yang, Q.; Zhang, Y.; Liu, J.; Gupta, U.; Subeta, V.; Sun, Y.; Sessi, P.; Parkin, S. S. P.; Bernevig, B. A.; Felser, C., Obstructed Surface States as the Descriptor for Predicting Catalytic Active Sites in Inorganic Crystalline Materials. *Adv Mater* **2022**, e2201328.

33. Eslami, M.; Zare, H. R.; Namazian, M., Thermodynamic Parameters of Electrochemical Oxidationof L-DOPA: Experimental and Theoretical Studies *J. Phys. Chem. B* **2012,** *116* (41), 12552–12557.

34. Ni, Z.; Wang, K.; Zhang, Y.; Pozo, O.; Xu, B.; Han, X.; Manna, K.; Paglione, J.; Felser, C.; Grushin, A. G.; de Juan, F.; Mele, E. J.; Wu, L., Giant topological longitudinal circular photo-galvanic effect in the chiral multifold semimetal CoSi. *Nat. Commun.* **2021,** *12* (1), 154.

35. Sun, Y.; Xu, Q.; Zhang, Y.; Le, C.; Felser, C., Optical method to detect the relationship between chirality of reciprocal space chiral multifold fermions and real space chiral crystals. *Phys. Rev. B* **2020,** *102* (10).
36. Lopez-Lozano, X.; Perez, L. A.; Garzon, I. L., Enantiospecific adsorption of chiral molecules on chiral gold clusters. *Phys. Rev. Lett.* **2006,** *97* (23), 233401.
37. Frazão, N. F.; Albuquerque, E. L.; Fulco, U. L.; Azevedo, D. L.; Mendonça, G. L. F.; Lima-Neto, P.; Caetano, E. W. S.; Santana, J. V.; Freire, V. N., Four-level levodopa adsorption on C60 fullerene for transdermal and oral administration: a computational study. *RSC Adv.* **2012,** *2* (22).
38. Chen, T.; Yang, H.; Yang, M.; Liu, F.; Wu, J.; Yang, S.; Wang, J., Controlling DOPA adsorption via interacting with polyelectrolytes: layer structure and corrosion resistance. *Soft Matter* **2020,** *16* (21), 4912-4918.
39. Rosenthal, D.; Widmer, R.; Wagner, R.; Gille, P.; Armbruster, M.; Grin, Y.; Schlogl, R.; Groning, O., Surface investigation of intermetallic PdGa(111). *Langmuir* **2012,** *28* (17), 6848-56.
40. Sigala, P. A.; Ruben, E. A.; Liu, C. W.; Piccoli, P. M.; Hohenstein, E. G.; Martinez, T. J.; Schultz, A. J.; Herschlag, D., Determination of Hydrogen Bond Structure in Water versus Aprotic Environments To Test the Relationship Between Length and Stability. *J Am. Chem. Soc.* **2015,** *137* (17), 5730-40.
41. Jiang, J.; Sun, F.; Zhou, S.; Hu, W.; Zhang, H.; Dong, J.; Jiang, Z.; Zhao, J.; Li, J.; Yan, W.; Wang, M., Atomic-level insight into super-efficient electrocatalytic oxygen evolution on iron and vanadium co-doped nickel (oxy)hydroxide. *Nat Commun* **2018,** *9* (1), 2885.
42. Naaman, R.; Paltiel, Y.; Waldeck, D. H., Chiral molecules and the electron spin. *Nat. Rev. Chem.* **2019,** *3* (4), 250-260.
43. Rogge, P. C.; Green, R. J.; Shafer, P.; Fabbris, G.; Barbour, A. M.; Lefler, B. M.; Arenholz, E.; Dean, M. P. M.; May, S. J., Inverted orbital polarization in strained correlated oxide films. *Phys. Rev B* **2018,** *98* (20).
44. Unzelmann, M.; Bentmann, H.; Figgemeier, T.; Eck, P.; Neu, J. N.; Geldiyev, B.; Diekmann, F.; Rohlf, S.; Buck, J.; Hoesch, M.; Kallane, M.; Rossnagel, K.; Thomale, R.; Siegrist, T.; Sangiovanni, G.; Sante, D. D.; Reinert, F., Momentum-space signatures of Berry flux monopoles in the Weyl semimetal TaAs. *Nat. Commun.* **2021,** *12* (1), 3650.
45. Gao, M.; Wang, Z.; Zhang, X.; Hao, X.; Qin, W., Spin-Photon Coupling in Organic Chiral Crystals. *Nano Lett* **2019,** *19* (12), 9008-9012.
46. Zhou, M.; Liu, K., Reactive resonance and the role of electron angular momentum. *Innovation* **2021,** *2* (3), 100136.